Hindawi Publishing Corporation
Shock and Vibration
Volume 2016, Article ID 8598749, 15 pages
http://dx.doi.org/10.1155/2016/8598749

Research Article

Effect of Hoisting Load on Transverse Vibrations of Hoisting Catenaries in Floor Type Multirope Friction Mine Hoists

Jiannan Yao and Xingming Xiao

School of Mechanical and Electrical Engineering, China University of Mining and Technology, Xuzhou 221116, China

Correspondence should be addressed to Xingming Xiao; xxm_cumt@126.com

Received 9 July 2015; Revised 22 October 2015; Accepted 27 October 2015

Academic Editor: Giorgio Dalpiaz

Copyright © 2016 J. Yao and X. Xiao. This is an open access article distributed under the Creative Commons Attribution License, which permits unrestricted use, distribution, and reproduction in any medium, provided the original work is properly cited.

The effect of hoisting load on transverse vibrations of hoisting catenaries during lifting in coal mines was investigated in this study. Firstly, dynamic analyses of the vertical hoisting rope were performed. The results show that transverse vibration plays the dominating role in the coupled dynamics of the vertical rope subjected to external excitation induced by axial fluctuations of head sheave, and the rope tension can be approximated by the quasistatic tension. Secondly, employing dynamic simulations, the effect of hoisting load on the transverse vibrations of hoisting catenaries was discussed. The results show that, under the second-order excitation frequency, a discrepant large transverse amplitude will be excited when the hoisting load ranges from 0 to 5000 kg, leading to collision between the two adjacent catenaries and accelerating the rupture of rope. To solve this problem, according to simulation curves, the self-weight of conveyance (preload) can be optimized from 39500 kg to 49500 kg. Eventually, on-site measurements were performed on the studied machine, validating the accuracy of the effect of hoisting load on transverse vibrations of hoisting catenaries. This investigation will greatly support facility maintenance, machine design, and even engineering optimization for floor type multirope friction mine hoists.

1. Introduction

Steel wire ropes are widely used in many industrial applications due to their high axial strength and bending flexibility [1]. In this latter application, cables connecting the mine hoist and the hoisting conveyance have played vital roles in mine hoisting systems because their endurance strength and fatigue life have great effect on the mine production and safety of miners [2]. A mine multirope hoisting system is shown in Figure 1. It comprises a driving friction pulley, four hoisting ropes, two sets of head sheaves, two skips, and three tail ropes. The four hoisting ropes pass from the same friction pulley over the four singular head sheaves to the skip constrained to move in a vertical shaft, forming four upper and lower catenaries and four vertical ropes.

Due to axial tensile loads and axial fluctuations of the head heaves, large amplitude transverse vibrations are usually associated with the hoisting catenaries as shown in Figure 2. The resonance may make two adjacent catenaries collide with each other and thereby accelerate the rupture of the rope.

In the dynamics of hoisting rope in mine hoists, some researchers have done some significant work in recent years. Cao et al. [3, 4] established the coupled extensional-torsional model for a frictional hoisting system with an oriented pulley and the extensional-torsional-lateral model for a winding hoisting system with a head heave. Wang et al. [5] investigated the lateral response of the moving hoisting conveyance in cable-guided hoisting system and revealed that the maximum lateral displacement is linearly proportional to the excitation amplitude. Goroshko [6] described the longitudinal-torsional vibrations of ropes, the elongation of which is obtained during untwisting and the twisting moment occurring under tension. Gong [7] proposed that resonance will be excited when an external excitation frequency approaches one mode of natural frequencies of the hoisting rope in a single-rope mine drum hoist; however, he did not study the influence factors. Kaczmarczyk [8] formulated an integral longitudinal model of the catenary-vertical hoisting cable system with a periodic excitation to analyze the passage through resonance. To investigate the dynamic behavior of a hoisting cable,

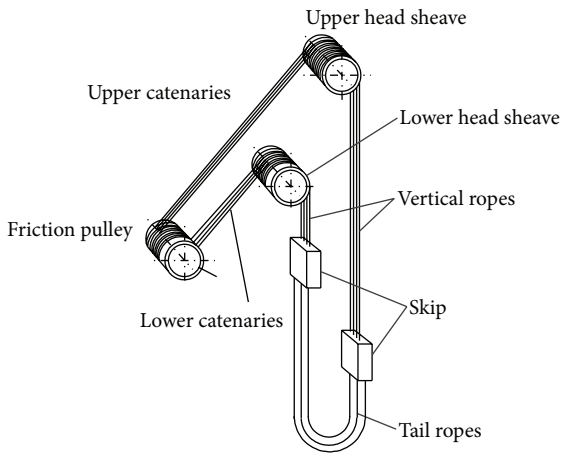

Figure 1: Schematic of a floor type multirope friction hoist in coal mine.

Kaczmarczyk and Ostachowicz [9, 10] derived a distributed-parameter mathematical model by employing the classical moving coordinate frame approach and Hamilton's principle with no regard to the transverse motions of head sheave in a single-rope mine drum hoist. Mankowski and Cox [11] studied the longitudinal response of mine hoisting cable to a kinetic shock load. Wang et al. [12] investigated the effect of terminal mass on fretting and fatigue parameters of the hoisting rope during a lifting cycle in coal mine.

From the literature studies mentioned above, few literatures have been focused on transverse vibrations of the hoisting catenaries in a multirope friction mine hoist with varying hoisting load. Therefore, the objective of the present study is to investigate the effect of hoisting load on the transverse vibrations of hoisting catenaries in a floor type multirope friction mine hoist. Firstly, the dynamics of the vertical translating hoisting rope, which can help explore the actual rope tension under different hoisting loads, was investigated. Secondly, theoretical correlation model between hoisting load and transverse vibrations of hoisting catenaries was established in order to study the influence of hoisting load on the transverse displacements of hoisting catenaries. Eventually, on-site measurements were carried out to validate the accuracy of the effect of hoisting load on the transverse displacements of hoisting catenary, and thereby the optimization of the hoisting load can be performed to reduce large amplitude transverse vibrations of the hoisting catenary.

2. Dynamics of Hoisting Rope Tension

Due to vibrations of the flexible vertically translating hoisting rope during lifting [13], dynamic analyses of the vertical translating hoisting rope can help to understand the actual rope tension and provide basic data for the analyses of transverse vibrations of hoisting catenaries.

2.1. Dynamic Model. To describe the dynamic behaviors of vertical hoisting ropes in colliery, assuming that the four vertical translating ropes have the same dynamic properties, only one rope was adopted as the study object and thereby a sliding coordinate system [14], oxy, was constructed as shown in Figure 3. Due to axial fluctuations of head sheaves, the transverse vibrations of vertical ropes are predominantly along the y direction in plane as shown in Figure 3. The hoisting rope has a time-varying length $l(t)$ at time instant t, a vertically translating velocity $v(t) = \dot{l}(t)$, acceleration $a(t) = \ddot{l}(t)$, and a total length L, where the overdot denotes time differentiation. The conveyance attached to the tip of the hoisting cable was modeled as a mass point with mass $m_e(t)$. The mass of the tail rope was integrated into mass of the conveyance. The displacement of the upper end of the cable, specified by $e(t)$, represents external excitation that is induced by the axial fluctuations of the head sheave. The transverse and longitudinal displacements of the rope particle instantaneously located in spatial position x at time t are represented by $y(x,t)$ and $w(x,t)$, respectively. $s(t)$ denotes the actual position of the sliding coordinate origin which represents the hoisting conveyance.

The equations governing the dynamic behavior of the translating cable [15] in Figure 3 in the x-y plane are

$$\begin{aligned}\rho\left(w_{tt}+aw_x+2vw_x+v^2w_{xx}+a\right)-T_x\left(1+w_x\right)\\ -Tw_{xx}-EA\left(w_{xx}+3w_xw_{xx}+1.5w_x^2w_{xx}\right.\\ \left.+0.5w_{xx}y_x^2+w_xy_xy_{xx}+y_xy_{xx}\right)=0,\\ 0\le x\le l(t),\end{aligned}\tag{1}$$

$$\begin{aligned}\rho\left(y_{tt}+ay_x+2vy_x+v^2y_{xx}\right)-T_xy_x-Ty_{xx}\\ -EA\left(y_xw_{xx}+1.5y_x^2y_{xx}+0.5y_{xx}w_x^2+y_xw_xw_{xx}\right.\\ \left.+y_{xx}w_x\right)=0,\quad 0\le x\le l(t),\end{aligned}\tag{2}$$

where the subscripts x and t denote partial differentiation; ρ, E, and A are the linear density, Young's modulus, and cross-sectional area of the hoisting rope, respectively; and $T(x,t)$ is the quasistatic tension in spatial position x at time t given by

$$T(x,t)=\left[m_e(t)+\rho x\right]\left[g+a(t)\right],\quad 0\le x\le l(t),\tag{3}$$

where g is the acceleration of gravity. Because the mass of the tail rope was integrated into the mass of the conveyance, hence the time-varying mass of the mass point in Figure 3 can be given by

$$m_e(t)=0.25\left[m_k+m_p+3\rho_t s(t)\right],\tag{4}$$

where the parameters m_k and m_p are relative to the mass of the conveyance and the actual hoisting load, respectively, and ρ_t denotes the linear density of the tail rope. The initial conditions of the cable are given by

$$\begin{aligned}w(x,0)=w_t(x,0)=y(x,0)=y_t(x,0)=0,\\ 0\le x\le l(0).\end{aligned}\tag{5}$$

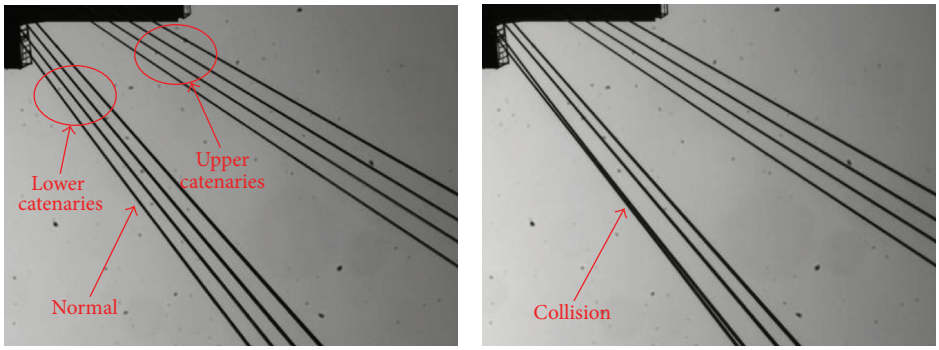

Figure 2: Diagram of collision behavior of hoisting catenaries.

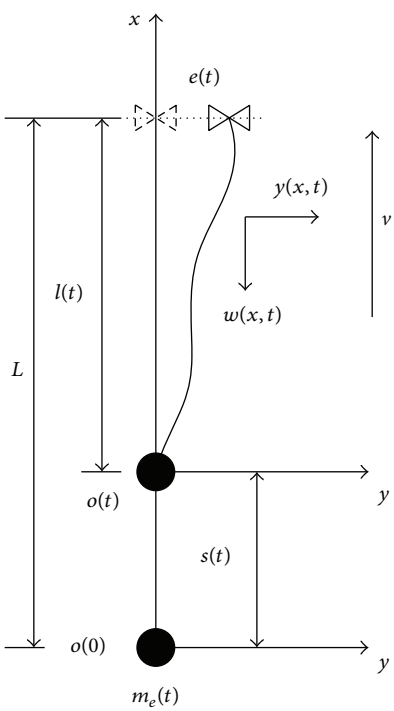

Figure 3: Diagram of hoisting rope in coal mine.

The boundary conditions of the vertical rope in Figure 3 are

$$\begin{aligned} w(0,t) &= w(l(t),t) = 0, \\ y(0,t) &= 0, \\ y(l(t),t) &= e(t). \end{aligned} \tag{6}$$

The governing equation in (2) with the time-dependent boundary conditions in (6) can be transformed to one with homogeneous boundary conditions. The transverse displacement is expressed in the form [16]

$$y(x,t) = u(x,t) + h(x), \tag{7}$$

where $u(x,t)$ and $h(x,t)$ are the parts that satisfy the corresponding homogeneous and nonhomogeneous boundary conditions, respectively. It is reasonable to assume that the lateral displacement from excitation varies from zero at the conveyance to $e(t)$ at the head sheave uniformly [15, 16]. Thus, the absolute displacement $h(x,t)$ can be defined to be a first-order polynomial in x and expressed as

$$h(x,t) = \frac{e(t)\,x}{l(t)}. \tag{8}$$

Substituting (6) into (2) yields

$$\begin{aligned} &\rho\left(u_{tt} + au_x + 2vu_x + v^2u_{xx}\right) - T_xu_x - Tu_{xx} \\ &\quad - EA\left(u_xw_{xx} + 1.5\left(u_x + h_x\right)^2\left(u_{xx} + h_{xx}\right)\right. \\ &\quad \left. + 0.5u_{xx}w_x^2 + u_xw_xw_{xx} + u_{xx}w_x\right) = f(x,t), \\ &\qquad\qquad 0 \le x \le l(t), \end{aligned} \tag{9}$$

where

$$\begin{aligned} &f(x,t) \\ &\quad = T_xh_x + Th_{xx} - \rho\left(h_{tt} + ah_x + 2vh_{xt} + v^2h_{xx}\right) \\ &\qquad + EA\left(h_xw_{xx} + 0.5h_{xx}w_x^2 + h_xw_xw_{xx} + h_{xx}w_x\right) \end{aligned} \tag{10}$$

is the additional forcing term induced by transforming the governing equation with time dependent nonhomogeneous boundary conditions to one with homogeneous boundary conditions. According to (6)-(7), the boundary conditions of the vertical rope in Figure 3 are

$$\begin{aligned} w(0,t) &= w(l(t),t) = 0, \\ u(0,t) &= 0, \\ u(l(t),t) &= 0, \\ h(0,t) &= 0, \\ h(l(t),t) &= e(t). \end{aligned} \tag{11}$$

2.2. Spatial Discretization. For simplicity, a new independent variable $\xi = x/l(t)$ was introduced, and the time-varying spatial domain $[0, l(t)]$ for x can be converted to a fixed domain $[0,1]$ for ξ. The new variables are $w^*(\xi,t) = w(x,t)$

and $u^*(\xi,t) = u(x,t)$, and the new variable for $h(x,t)$ is $h^*(\xi,t)$. The partial derivatives of $w(x,t)$ and $u(x,t)$ with respect to x and t relative to those of $w^*(\xi,t)$ and $u^*(\xi,t)$ with respect to ξ and t are

$$\begin{aligned} w_x &= l^{-1}(t)\, w^*_\xi, \\ w_{xx} &= l^{-2}(t)\, w^*_{\xi\xi}, \\ w_t &= w^*_t - \xi v l^{-1}(t)\, w^*_\xi, \\ w_{xt} &= l^{-1}(t)\, w^*_{\xi t} - v l^{-2}(t)\, w^*_\xi - \xi v l^{-2}(t)\, w^*_{\xi\xi}, \\ w_{tt} &= w^*_{\xi\xi} - 2\xi v l^{-1}(t)\, w^*_{\xi t} + \xi^2 v^2 l^{-2}(t)\, w^*_{\xi\xi} \\ &\quad - \left[a l(t) - 2v^2\right] \xi l^{-2}(t)\, w^*_\xi, \end{aligned} \tag{12}$$

$$\begin{aligned} u_x &= l^{-1}(t)\, u^*_\xi, \\ u_{xx} &= l^{-2}(t)\, u^*_{\xi\xi}, \\ u_t &= u^*_t - \xi v l^{-1}(t)\, u^*_\xi, \\ u_{xt} &= l^{-1}(t)\, u^*_{\xi t} - v l^{-2}(t)\, u^*_\xi - \xi v l^{-2}(t)\, u^*_{\xi\xi}, \\ u_{tt} &= u^*_{\xi\xi} - 2\xi v l^{-1}(t)\, u^*_{\xi t} + \xi^2 v^2 l^{-2}(t)\, u^*_{\xi\xi} \\ &\quad - \left[a l(t) - 2v^2\right] \xi l^{-2}(t)\, u^*_\xi, \end{aligned} \tag{13}$$

where the subscript ξ denotes partial differentiation. Similarly, the partial derivatives of $h(x,t)$ versus x and t are expressed as

$$\begin{aligned} h_x &= l^{-1}(t)\, h^*_\xi, \\ h_{xx} &= l^{-2}(t)\, h^*_{\xi\xi}, \\ h_t &= h^*_t - \xi v l^{-1}(t)\, h^*_\xi, \\ h_{xt} &= l^{-1}(t)\, h^*_{\xi t} - v l^{-2}(t)\, h^*_\xi - \xi v l^{-2}(t)\, h^*_{\xi\xi}, \\ h_{tt} &= h^*_{\xi\xi} - 2\xi v l^{-1}(t)\, h^*_{\xi t} + \xi^2 v^2 l^{-2}(t)\, h^*_{\xi\xi} \\ &\quad - \left[a l(t) - 2v^2\right] \xi l^{-2}(t)\, h^*_\xi, \end{aligned} \tag{14}$$

where the terms about h^* are given as follows:

$$\begin{aligned} h^*_\xi &= e(t), \\ h^*_t &= \xi \dot{e}(t), \\ h^*_{\xi t} &= \dot{e}(t), \\ h^*_{\xi\xi} &= 0, \\ h^*_{tt} &= \xi \ddot{e}(t). \end{aligned} \tag{15}$$

Substituting (3), (13), and (14) into (9)and omitting the high-order terms [16] yield

$$\begin{aligned} &\rho \left\{ u^*_{tt} + 2v l^{-1}(t)(1-\xi)\, u^*_{\xi t} + v^2 l^{-2}(t)(1-\xi)^2\, u^*_{\xi\xi} \right. \\ &\quad \left. + \left[a l(t) - 2v^2 l^{-2}(t)\right](1-\xi)\, u^*_\xi \right\} - \rho(g+a)\, l^{-1}(t) \\ &\quad \cdot u^*_\xi - \left[m_e(t) + \rho\xi l(t)\right](g+a)\, l^{-2}(t)\, u^*_{\xi\xi} \\ &\quad - 1.5 E A l^{-4}(t)\, u^*_{\xi\xi} {h^*_\xi}^2 = f_{\mathrm{tr}}(\xi,t), \quad 0 \le \xi \le 1, \end{aligned} \tag{16}$$

where

$$\begin{aligned} f_{\mathrm{tr}}(\xi,t) &= -\rho \left\{ h^*_{tt} + 2v l^{-1}(t)\, h^*_{\xi t} \right. \\ &\quad \left. + \left[a l^{-1}(t) - 2v^2 l^{-2}(t)\right](1-\xi)\, h^*_\xi \right\} + \rho(g+a) \\ &\quad \cdot l^{-1}(t)\, h^*_\xi + E A l^{-3}(t)\, h^*_\xi w^*_{\xi\xi}. \end{aligned} \tag{17}$$

Substituting (12) into (1) and omitting the high-order terms yield

$$\begin{aligned} &\rho \left\{ w^*_{tt} + 2v l^{-1}(t)(1-\xi)\, w^*_{\xi t} + v^2 l^{-2}(t)(1-\xi)^2\, w^*_{\xi\xi} \right. \\ &\quad \left. + \left[a l(t) - 2v^2 l^{-2}(t)\right](1-\xi)\, w^*_\xi \right\} - \rho(g+a)\, l^{-1}(t) \\ &\quad \cdot w^*_\xi - \left[m_e(t) + \rho\xi l(t)\right](g+a)\, l^{-2}(t)\, w^*_{\xi\xi} \\ &\quad - E A \left\{ \left[l^{-2}(t) + 2 l^{-4}(t) {h^*_\xi}^2 \right] w^*_{\xi\xi} + l^{-2}(t)\, h^*_\xi w^*_\xi \right\} \\ &\quad = f_{\mathrm{lon}}(\xi,t), \quad 0 \le \xi \le 1, \end{aligned} \tag{18}$$

where

$$f_{\mathrm{lon}}(\xi,t) = \rho g + E A l^{-3}(t)\, h^*_\xi u^*_\xi. \tag{19}$$

Galerkin method could be used to transform (16) and (18) into a set of ordinary differential equations by separating the transverse displacement as

$$\begin{aligned} w(\xi,t) &= l^{-0.5}(t) \sum_{i=1}^{n} U_i(\xi)\, p_i(t), \\ u(\xi,t) &= l^{-0.5}(t) \sum_{i=1}^{n} U_i(\xi)\, q_i(t), \end{aligned} \tag{20}$$

where n represents the order of the mode, $p_i(t)$ and $q_i(t)$ are the generalized coordinates, and the mode shape is

$$U_i(\xi) = \sqrt{2} \sin\left(\frac{2i-1}{2}\pi\xi\right). \tag{21}$$

Substituting (20) into (16) and (18), then multiplying (16) and (18) by $U_j(\xi) l^{-0.5}(t)$, $(j = 1, 2, \ldots, n)$, and integrating (16) and (18) over the interval of 0 and 1, ordinary differential equations can be obtained as

$$\begin{aligned} &\begin{bmatrix} M_{\mathrm{lon}} & 0 \\ 0 & M_{\mathrm{tr}} \end{bmatrix} \begin{bmatrix} \ddot{P} \\ \ddot{Q} \end{bmatrix} + \begin{bmatrix} C_{\mathrm{lon}} & 0 \\ 0 & C_{\mathrm{tr}} \end{bmatrix} \begin{bmatrix} \dot{P} \\ \dot{Q} \end{bmatrix} \\ &\quad + \begin{bmatrix} K_{\mathrm{lon}} & 0 \\ 0 & K_{\mathrm{tr}} \end{bmatrix} \begin{bmatrix} P \\ Q \end{bmatrix} + \begin{bmatrix} CP_{\mathrm{lon}} \\ CP_{\mathrm{tr}} \end{bmatrix} = \begin{bmatrix} F_{\mathrm{lon}} \\ F_{\mathrm{tr}} \end{bmatrix}, \end{aligned} \tag{22}$$

where $P = [p_1, p_2, \ldots, p_n]^T$ and $Q = [q_1, q_2, \ldots, q_n]^T$ are the vectors of generalized coordinates and M $(M_{\text{lon}}, M_{\text{tr}})$, C $(C_{\text{lon}}, C_{\text{tr}})$, K $(K_{\text{lon}}, K_{\text{tr}})$, and F $(F_{\text{lon}}, F_{\text{tr}})$ are the mass, damping, stiffness matrices, and the force vector, respectively, and CP $(CP_{\text{lon}}, CP_{\text{tr}})$ is the coupled term. Entries of these matrices are formulated as

$$\begin{aligned}
M_{\text{lon}.ij} &= M_{\text{tr}.ij} = \delta_{ij},\\
C_{\text{lon}.ij} &= C_{\text{tr}.ij} = -vl^{-1}(t)\,\delta_{ij} + 2vl^{-1}(t)\int_0^1 (1-\xi)\\
&\quad \cdot U_i'(\xi)\,U_j(\xi)\,d\xi,\\
K_{\text{lon}.ij} &= \left[0.75v^2l^{-2}(t) - 0.5al^{-1}(t)\right]\delta_{ij} + v^2l^{-2}(t)\\
&\quad \cdot \int_0^1 (1-\xi)^2 U_i''(\xi)\,U_j(\xi)\,d\xi + \left[3v^2l^{-2}(t)\right.\\
&\quad \left. - al^{-1}(t)\right]\int_0^1 (\xi-1)\,U_i'(\xi)\,U_j(\xi)\,d\xi - \left[(g+a)\right.\\
&\quad \left. \cdot l^{-1}(t) + EAe(t)\,\rho^{-1}l^{-2}(t)\right]\int_0^1 U_i'(\xi)\,U_j(\xi)\,d\xi\\
&\quad - \left[m_e(t)(g+a)\,\rho^{-1}l^{-2}(t) + EA\rho^{-1}l^{-2}(t)\right.\\
&\quad \left. + 0.5EAe^2(t)\,\rho^{-1}l^{-4}(t)\right]\int_0^1 U_i''(\xi)\,U_j(\xi)\,d\xi - (g\\
&\quad + a)\,l^{-1}(t)\int_0^1 \xi U_i''(\xi)\,U_j(\xi)\,d\xi,\\
K_{\text{tr}.ij} &= \left[0.75v^2l^{-2}(t) - 0.5al^{-1}(t)\right]\delta_{ij} + v^2l^{-2}(t)\\
&\quad \cdot \int_0^1 (1-\xi)^2 U_i''(\xi)\,U_j(\xi)\,d\xi + \left[3v^2l^{-2}(t)\right.\\
&\quad \left. - al^{-1}(t)\right]\int_0^1 (\xi-1)\,U_i'(\xi)\,U_j(\xi)\,d\xi - \left[(g+a)\right.\\
&\quad \left. \cdot l^{-1}(t)\right]\int_0^1 U_i'(\xi)\,U_j(\xi)\,d\xi - \left[m_e(t)(g+a)\right.\\
&\quad \left. \cdot \rho^{-1}l^{-2}(t) + 1.5EAe^2(t)\,\rho^{-1}l^{-4}(t)\right]\int_0^1 U_i''(\xi)\\
&\quad \cdot U_j(\xi)\,d\xi - (g+a)\,l^{-1}(t)\int_0^1 \xi U_i''(\xi)\\
&\quad \cdot U_j(\xi)\,d\xi,\\
CP_{\text{lon}.ij} &= -EAe(t)\,q_i(t)\,\rho^{-1}l^{-3}(t)\int_0^1 U_i''(\xi)\,U_j(\xi)\,d\xi,\\
CP_{\text{tr}.ij} &= -EAp_i(t)\,\rho^{-1}l^{-3}(t)\int_0^1 U_i''(\xi)\,U_j(\xi)\,d\xi,\\
F_{\text{lon}.j} &= l^{0.5}(t)\,g\int_0^1 U_j(\xi)\,d\xi,\\
F_{\text{tr}.j} &= -l^{0.5}(t)\int_0^1 \left\{\left[al^{-1}(t) - 2v^2l^{-2}(t)\right]e(t)(1-\xi)\right.\\
&\quad \left. - (g+a)\,l^{-1}(t)\,e(t) + \xi\ddot{e}(t) + 2\dot{e}(t)\,vl^{-1}(t)\right\}\\
&\quad \cdot U_j(\xi)\,d\xi,
\end{aligned} \tag{23}$$

where δ_{ij} is the Kronecker delta defined by $\delta_{ij} = 1$ if $i = j$ and $\delta_{ij} = 0$ if $i \neq j$.

2.3. Hoisting Rope Tension. The dynamic tension at the particle located in spatial position x at time t is [17]

$$P(x,t) = T(x,t) + EA\varepsilon(x,t), \tag{24}$$

where $T(x,t)$ and $EA\varepsilon(x,t)$ are the quasistatic and vibratory axial forces at the particle with the coordinate x at time t, respectively, and $\varepsilon(x,t)$ is the strain in spatial position x at time t which can be approximated as [18]

$$\varepsilon(x,t) = w_x(x,t) + 0.5w_x^2(x,t) + 0.5y_x^2(x,t). \tag{25}$$

Dynamic responses were calculated for a vertical hoisting rope in a multirope friction mine hoist. The parameters for the model shown in Figure 3 were $\rho = 7.86$ m/s, $\rho_t = 10.48$ m/s, $EA = 1.5246 \times 10^8$ N/m, and $m_k = 39500$ kg. The rope is assumed to be at rest initially; hence $y(x,0) = y_t(x,0) = w(x,0) = w_t(x,0) = 0$. Consider the upward movement profile in Figure 4, which is divided into three stages. The velocity function $v(t)$ is given by the following formula:

$$v_i(t) = v_{0i} + a_i\Delta t_i, \quad (i = 1, 2, 3), \tag{26}$$

where the initial velocities at the 1st to 3rd stage, v_{01} to v_{03}, are 0, 9.31 m/s, and 9.31 m/s, respectively; the accelerations at the 1st to 3rd stage are 0.7 m/s^2, 0, and −0.7 m/s^2, respectively; the hoisting time at the 1st stage is 13.3 s, and 59.4 s and 13.3 s correspond to the 2nd and 3rd stages. The maximum velocity and acceleration are 9.31 m/s and 0.7 m/s^2, respectively, and the total travel time is 86 s. According to the time-varying lengths of the tail rope and the vertical rope shown in Figures 4(a) and 4(b), the initial and final lengths of the vertical rope are 699 m and 22 m, respectively, and the initial and final lengths of the tail rope are 14 m and 691 m, respectively.

The boundary excitations are induced by axial fluctuations of head sheaves specified by $e(t) = A\sin(wt)$, where $A = 0.005$ m and $w = n \times 2v(t)/D$. D, the diameter of the head sheave, has a value of 4.5 m. Applying the conclusion in reference [19] that the first three-order frequency components play the dominating roles in the axial fluctuations of head sheaves in mine hoists, hence, $n = 1, 2, 3$. The transverse displacements at the sheave end, which also act as the external displacement excitations, are demonstrated in Figure 5.

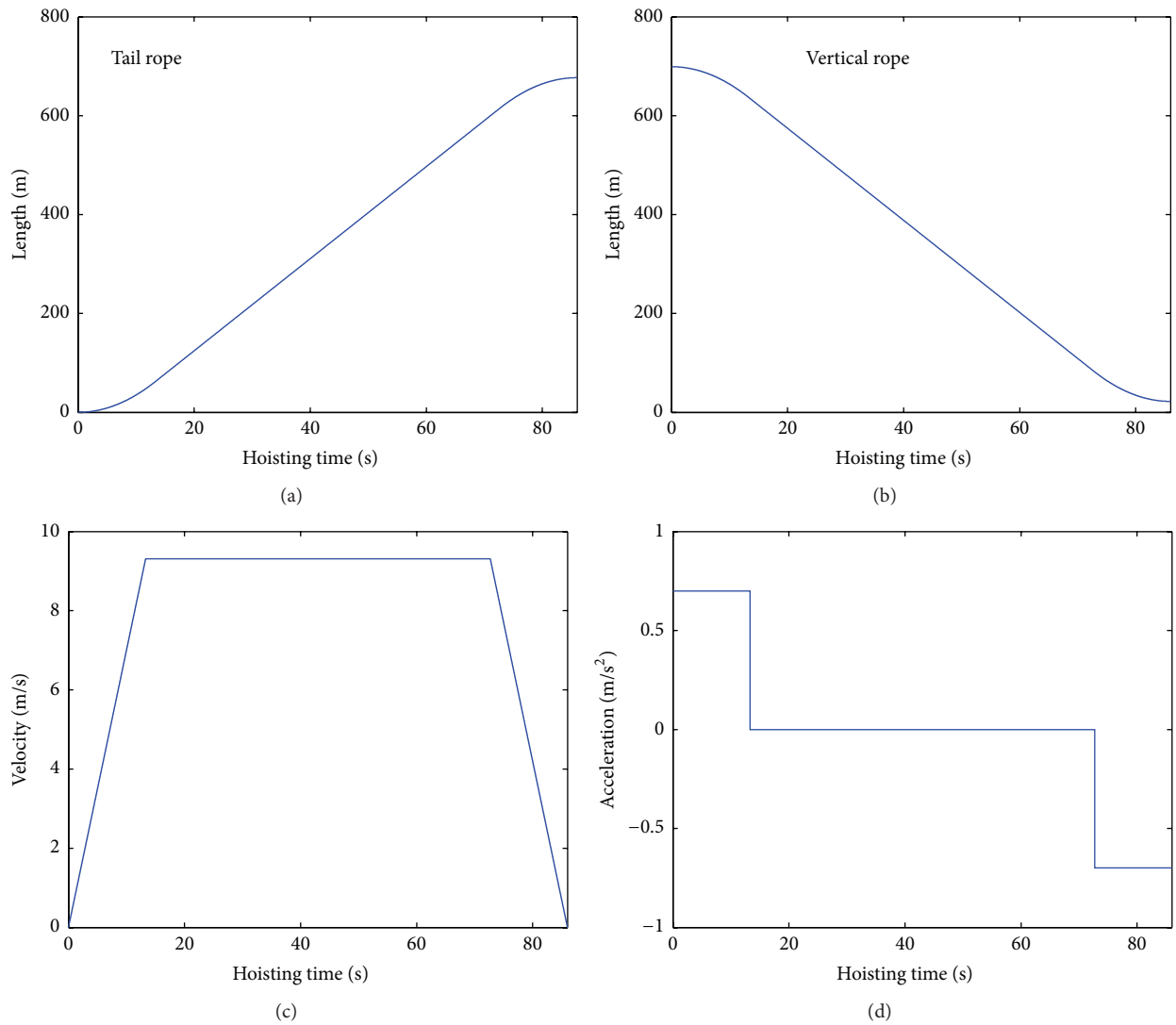

Figure 4: Upward movement profile of the conveyance: (a) time-varying length of the tail rope; (b) time-varying length of the vertical rope; (c) hosting velocity; (d) hoisting acceleration.

To obtain the rope tension at the sheave end, according to (24)-(25), the dynamic strains at the sheave end should be calculated firstly and can be expressed as

$$\begin{aligned} w_{l(t)}(l(t),t) &= l^{-1.5}(t)\sum_{i=1}^{10}\sqrt{2}\frac{2i-1}{2}\pi\cos\left(\frac{2i-1}{2}\pi\right)p_i(t), \\ y_{l(t)}(l(t),t) &= \frac{e(t)}{l(t)}, \\ \varepsilon(l(t),t) &= w_{l(t)}(l(t),t)+0.5w_{l(t)}^2(l(t),t) \\ &\quad + 0.5y_{l(t)}^2(l(t),t). \end{aligned} \tag{27}$$

Under the above external displacement excitations, the longitudinal and transverse strains at the top of the vertical rope (sheave end, $x = l(t)$) were calculated as shown in Figures 6 and 7. The convergence of (22) can be examined by varying the number of included modes. In this case, the number of included modes can be determined as 10.

It can be inferred from Figures 6 and 7 that, under the 1st- to 3rd-order excitations, the longitudinal strains at the sheave end are far less than the transverse no matter with full load or no load. Hence, it can be concluded that the transverse strain plays the dominating role in the coupled dynamics of the vertical hoisting rope. According to (27), the length of the vertical rope, $l(t)$, and its exponent were used as the main divisor which can make the dynamic strain of the rope at the sheave end so small. For example, according to (27), the transverse strain at the sheave end can be expressed as $0.5(e(t)/l(t))^2$ and the range of $e(t)$ is -0.005 m to 0.005 m which is far less than the range of the length of the vertical

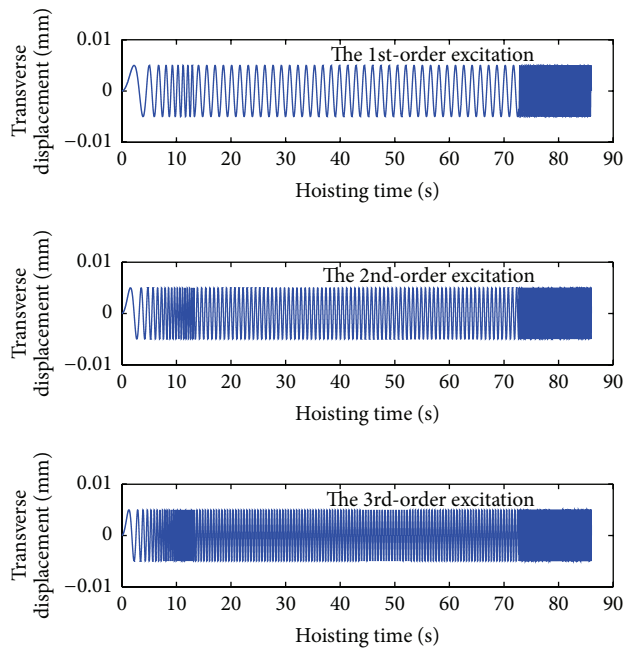

Figure 5: The transverse displacements at the sheave end with different orders.

rope (22 m to 699 m); therefore, it accounts for such small dynamic strain at the sheave end. Additionally, there is no obvious difference between the responses of the dynamic strain under the 1st- to 3rd-order excitations. Therefore, there is no dominant frequency of the oscillation. Applying (24), the quasistatic and vibratory axial force at the sheave end during the hoisting process can be obtained as shown in Figure 8. It can be noted that the vibratory axial force at the sheave end is much smaller than the quasistatic, no matter whether under the condition of no or full hoisting load. Hence, the tension in the vertical rope can be approximated by the quasistatic tension.

3. Effect of Hoisting Load on Transverse Vibrations of Hoisting Catenaries

The hoisting catenaries in a multirope friction mine hoist are typically moving cables with constant length and usually suffer intense transverse vibrations induced by axial fluctuations of head sheaves. As shown in Figures 2 and 9, large amplitude transverse vibrations will contribute to collision between two adjacent catenaries, accelerating the rupture of the rope. In the present work, the effect of hoisting load on transverse vibrations of catenaries was investigated.

3.1. Dynamic Model. To describe the transverse vibrations of hoisting catenaries, a fixed coordinate system, *oxy*, is established. Due to axial fluctuations of head sheaves, the transverse vibrations of catenaries are predominantly along the y direction in plane as shown in Figure 9. The four catenaries wrap around the same friction pulley and attach to the four singular sheaves, respectively. In the present study, only one catenary was adopted to conduct the research for simplicity. The friction pulley is modeled as a fixed-center pulley, and the singular head sheave is modeled as a point subjected to axial fluctuating displacement specified by $e(t)$, where t is the hoisting time.

The transverse displacement of the catenary in the position x at time t, $y_c(x,t)$, has been derived in our previous work [19]; its governing equation can be expressed as

$$\frac{\partial^2 y_c(x,t)}{\partial t^2} + a(t)\frac{\partial y_c(x,t)}{\partial x} + 2v(t)\frac{\partial^2 y_c(x,t)}{\partial t \partial x} + \left(v^2(t) - \frac{T_c(x,t)}{\rho}\right)\frac{\partial^2 y_c(x,t)}{\partial x^2} = 0, \tag{28}$$

in which $a(t)$ and $v(t)$ are the hoisting acceleration and velocity, respectively; ρ is the linear density of the hoisting rope; and $T_c(x,t)$ is the axial tension of the catenary located in position x at time t. Due to the continuity of deflection across the head sheave, it is required that the dynamic tension in the catenary equals that at the top of the vertical rope [9] as shown in Figure 8. What is more, the effect of gravity due to a catenary inclination is small compared to the total quasistatic tension; hence, the effect of gravity can be omitted and thereby the axial tension in each point of the catenary can be approximated identically. Consequently, the axial tension in the catenary can be expressed as

$$T_c(t) = P(l(t),t) = T(l(t),t) + EA\varepsilon(l(t),t). \tag{29}$$

Applying the conclusion in Section 2.3 that the tension in the vertical rope can be approximated by the quasistatic tension, hence, according to (3)-(4), the axial tension in the catenary can be derived as

$$T_c(t) = \left[0.25m_k + 0.25m_p + \rho L\right]\left[g + a(t)\right]. \tag{30}$$

Assume that the transverse displacement of a catenary can be expressed as

$$y_c(x,t) = \sum_{n=1}^{2} q_n(t)\sin\left(n\pi x L_c^{-1}\right) + \xi e(t), \qquad \xi = \frac{x}{L_c}\ (x = 0 \sim L_c), \tag{31}$$

where $q_n(t)$ is a set of generalized displacements of the catenary and $\sin(n\pi\xi)$ is a set of trial functions; L_c is the constant length of the catenary. Substituting (31) into (28) yields

$$\begin{aligned} R(\xi,t) = {} & \sum_{n=1}^{2}\ddot{q}_n(t)\sin(n\pi\xi) \\ & + \frac{\pi}{L_c}a(t)\sum_{n=1}^{2} n q_n(t)\cos(n\pi\xi) \\ & + \frac{2\pi v(t)}{L_c}\sum_{n=1}^{2} n\dot{q}_n(t)\cos(n\pi\xi) \\ & - \frac{\pi^2 L_c^2}{v^2(t) - T_c(x,t)\rho^{-1}}\sum_{n=1}^{2} n^2 q_n(t)\sin(n\pi\xi). \end{aligned} \tag{32}$$

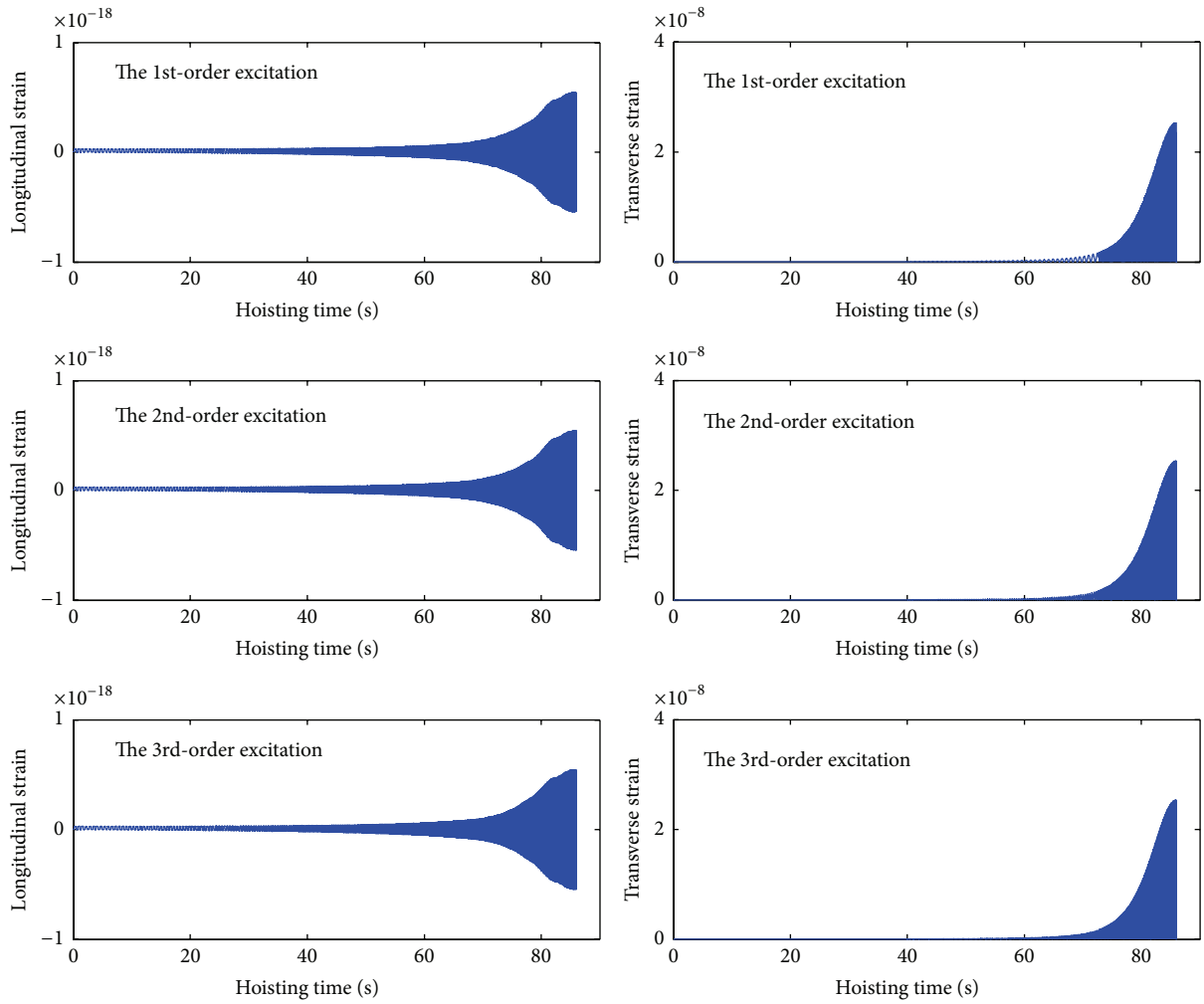

Figure 6: The longitudinal and transverse strains at the sheave end under the condition of no hoisting load, $m_p = 0$.

According to Galerkin method, the requirement is

$$\int_0^1 R(\xi, t) \sin(j\pi\xi)\, d\xi = 0, \quad (j = 1, 2). \tag{33}$$

Inserting (32) into (33) and integrating the resulting equation yield the simplified equations of motion:

$$\begin{aligned}\ddot{q}_1(t) &= \frac{8}{3} a(t) L_c^{-1} q_2(t) + \frac{16}{3} v(t) L_c^{-1} \dot{q}_2(t) \\ &\quad + \pi^2 L_c^{-2} \left[v^2(t) - T_c(x,t)\rho^{-1}\right] q_1(t) \\ &\quad - \left[4\pi^{-1} L_c^{-1} a(t) e(t) + 8v(t)\pi^{-1} L_c^{-1} \dot{e}(t) \right. \\ &\quad \left. - 2\pi^{-1} \ddot{e}(t)\right], \\ \ddot{q}_2(t) &= -\frac{8}{3} a(t) L_c^{-1} q_1(t) - \frac{16}{3} v(t) L_c^{-1} \dot{q}_1(t) \\ &\quad + 4\pi^2 L_c^{-2} \left[v^2(t) - T_c(x,t)\rho^{-1}\right] q_2(t) + \pi^{-1} \ddot{e}(t).\end{aligned} \tag{34}$$

3.2. Transverse Vibrations of the Catenary with Varying Hoisting Load. In this section, the maximum transverse amplitudes at the center of the lower catenary with varying hoisting load are simulated. The fluctuating displacement of the head sheave can be specified by $e(t) = A\sin(nwt)$, where $w = 2v(t)/D$ is the rotational frequency of the head sheave; $v(t)$ is the hoisting speed in Figure 4(c); D, the diameter of the head sheave, has a value of 4.5 m; and n is the number of the included order. According to the conclusion mentioned in [19] that the first three-order frequency components play the dominating roles in the axial fluctuations of head sheaves, therefore, $n = 3$. The constant length of the lower catenary, Lc, is 43.88 m, and the other parameters are the same as those introduced in Section 2.3. Finally, according to (31), the effects of hoisting load on transverse vibrations can be investigated as shown in Figures 10, 11, and 12, respectively.

It can be seen from Figures 10, 11, and 12 that the maximum amplitude at the center of the catenary increases with the increasing excitation amplitude. When the excitation amplitude is constant, with varying hoisting load under the first- and third-order excitation frequency, the maximum

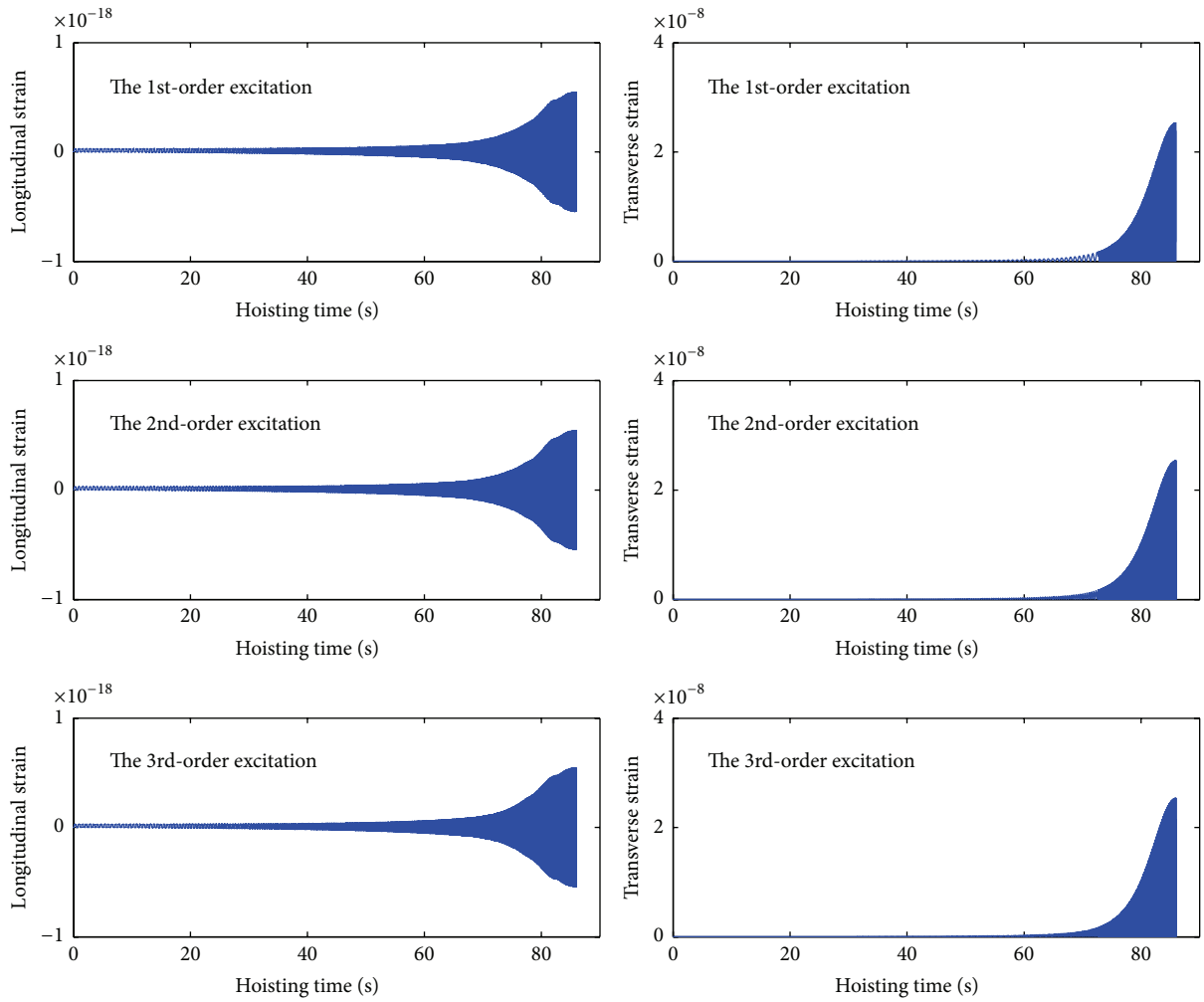

FIGURE 7: The longitudinal and transverse strains at the sheave end under the condition of full hoisting load, $m_p = 20000$ kg.

amplitude changes smoothly and has relatively small value that is less than 35 mm. However, as shown in Figure 11, under the second-order excitation frequency, a discrepant large transverse amplitude emerges when the hoisting load is within the range from 0 to 5000 kg. In this study, the rope spacing between two adjacent catenaries in the multirope friction mine hoist has a constant value of 350 mm. Therefore, if the maximum transverse amplitudes of two adjacent catenaries both exceed the dangerous threshold of 175 mm, collision between the two adjacent catenaries will result as shown in Figure 2, accelerating the rupture of the rope. Especially in the case that the hoisting load is about 2500 kg, even the excitation amplitude is as small as 1 mm and the maximum transverse amplitude under the second-order excitation frequency has exceeded the dangerous threshold of 175 mm, which is strictly prohibited in the industrial field of coal mines.

To guarantee the safety production in coal mines, large amplitude transverse vibrations must be avoided. The mine hoist mainly operates under two working conditions, that is, no hoisting load with $m_p = 0$ and full hoisting load with $m_p = 20000$ kg in this case. The self-weight of the conveyance (preload) in this case is $m_k = 39500$ kg. Hence, to avoid the discrepant large transverse amplitude, the self-weight of the conveyance (preload) can be optimized from 39500 kg to 49500 kg by adding 10000 kg, equal to transforming the original hoisting load range [0, 20000 kg] to a new range [10000 kg, 30000 kg] as shown in Figure 11. Eventually, the discrepant large transverse amplitude and the collision between two adjacent catenaries can be thoroughly avoided, making the mine hoist operate in stability.

However, at the same time, it should be noted that increasing preload leads to higher mean stress which certainly in turn affects fatigue life of the rope. The JKMD-4.5 × 4(III) E floor type multirope friction mine hoist is the machine that the present work is focusing on, and the permitted maximum tension of a rope in this machine is 900 KN. Before optimization, according to (30), the maximum tension of a rope during the hoisting process with full load is 213.88 KN, and the corresponding rope tension is 240.13 KN after increasing the preload by 10000 kg. The maximum optimized rope tension, 240.13 KN, is still far less than the permitted, 900 KN. There is no doubt that increasing the rope tension will shorten the fatigue life of

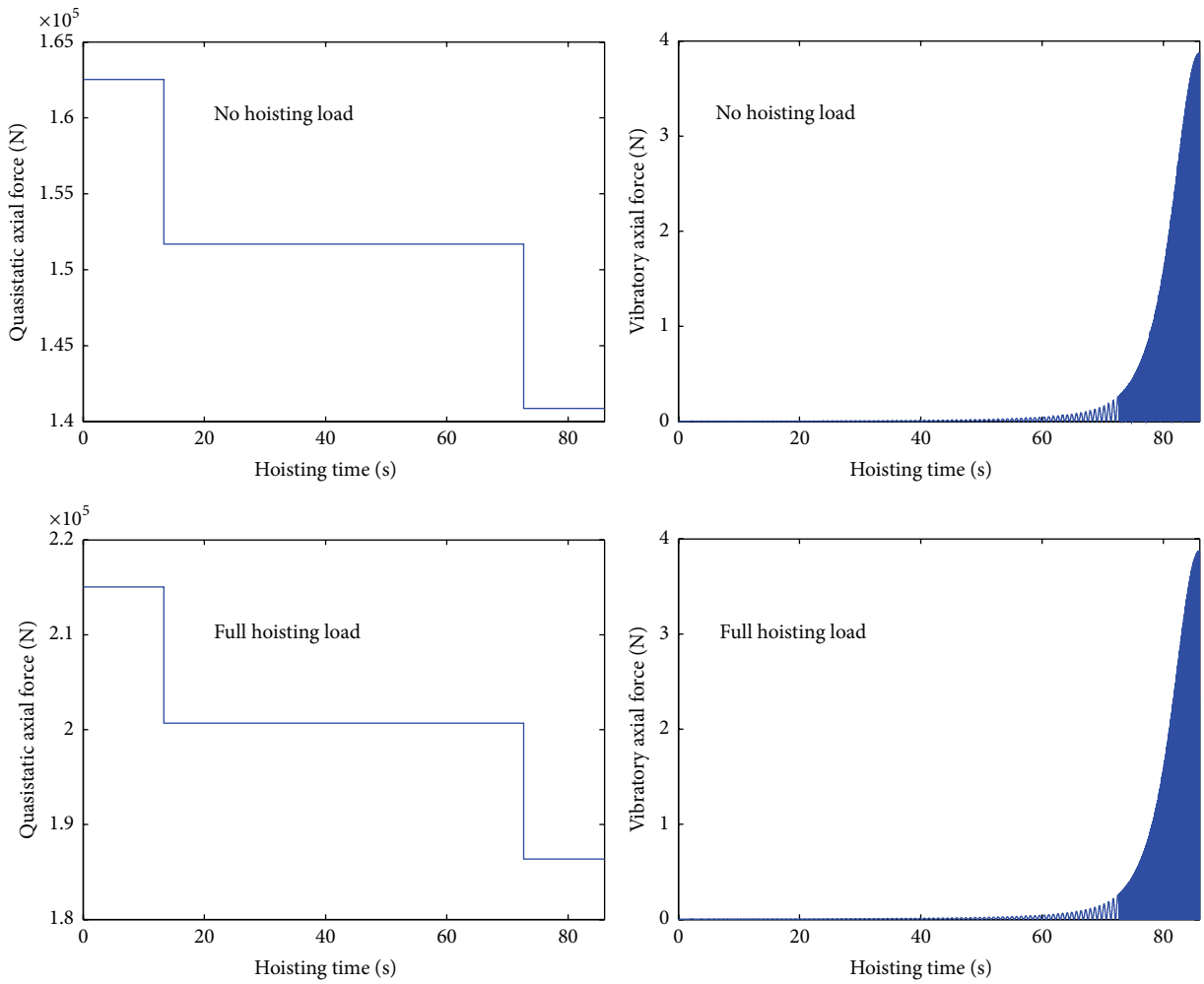

Figure 8: The quasistatic and vibratory axial force at the sheave end during the hoisting process.

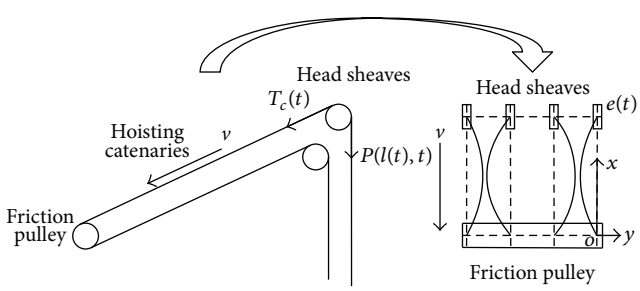

Figure 9: Diagram of the transverse vibration model of hoisting catenaries.

a rope; however, if collision between two adjacent catenaries occurs because of resonance as shown in Figure 11, though the fatigue life of ropes may be shortened, increasing preload can rapidly avoid resonance and still make the machine operate in safety for a long time. Therefore, increasing preload is still an acceptable method to rapidly remove the collision between catenaries. Furthermore, the proposed technique can also help the engineers to choose reasonable hoisting parameters in the design phase of the machine to avoid potential failures.

4. Measurement and Validation

4.1. On-Site Measurements. During the hoisting process as shown in Figure 4, real object tests were performed on the studied multirope friction hoist in the Yaoqiao Coal Mine of Shanghai Datun Joint Co. Ltd.

In the present work, lower catenary 4 was adopted as the study object for simplicity. Hence, to obtain the transverse displacements of the center point of lower catenary 4, a high-speed camera, which was placed beneath the moving catenaries at an arbitrary appropriate distance, was applied to record the sequential images during the hoisting process with no and full hoisting load, respectively. The processed image was shown in Figure 13. A guide line, which was perpendicular to the hoisting catenaries, was first inserted in the sequential images. Then, at the start frame in which the static equilibrium catenary was recorded, a tracking window was defined in the intersection area of lower catenary 4 and the guide line. To calculate the actual vibration displacement,

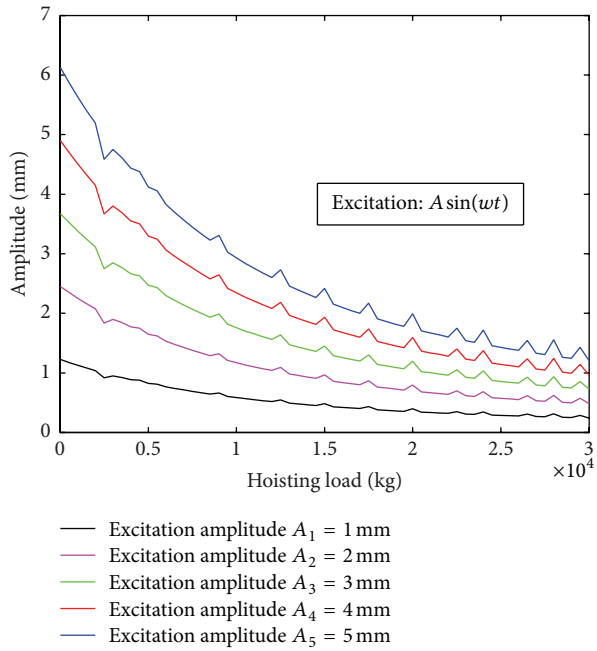

Figure 10: Maximum amplitude at the center of the catenary under the first-order excitation angular frequency with varying hoisting load.

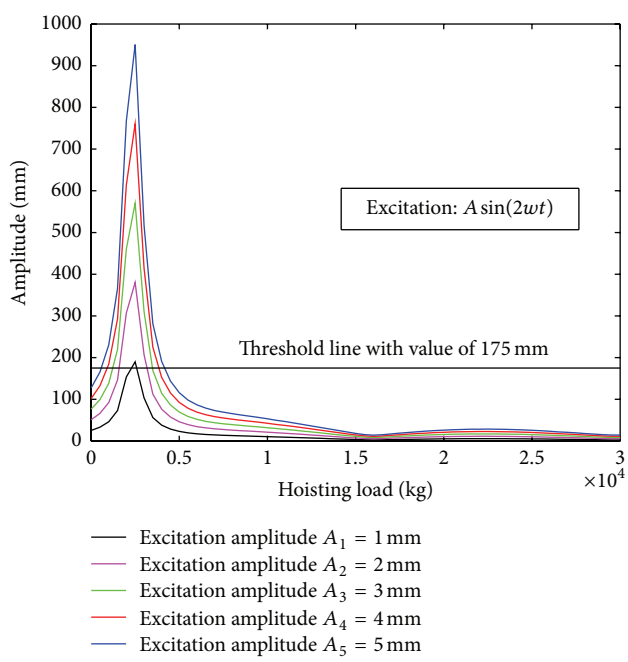

Figure 11: Maximum amplitude at the center of the catenary under the second-order excitation angular frequency with varying hoisting load.

it is imperative to obtain the scaling factor λ. The length of line ab in Figure 13(b) is relative to the rope spacing which has a constant value of 350 mm. The coordinates of points a and b are $(544, 747)$ and $(650, 718)$, respectively. And the pixel distance of line ab can be calculated as 109.9. Thus, the scaling factor λ can be calculated as 3.18 mm/pixel.

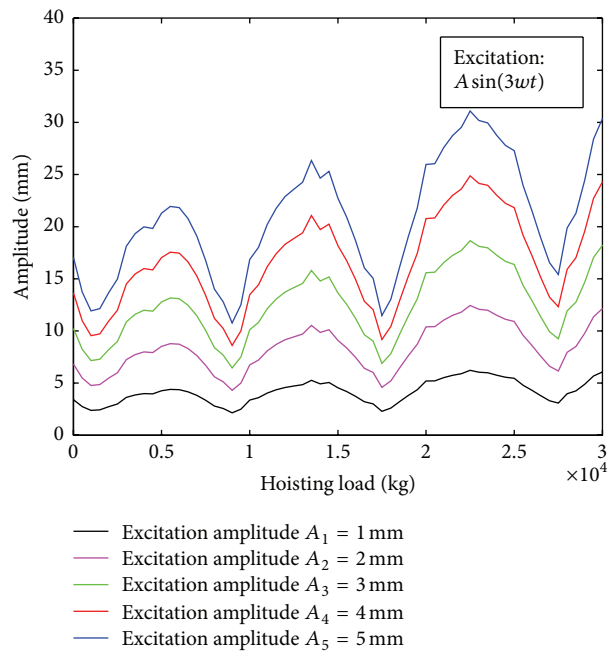

Figure 12: Maximum amplitude at the center of the catenary under the third-order excitation angular frequency with varying hoisting load.

Eventually, through tracking the dynamic intersection area by employing mean shift tracking algorithm [20–22] and then recording the location of the tracker, the transverse vibration displacements of the center point of the lower hoisting catenary 4 can be obtained as demonstrated in Figure 14.

During the measurement of transverse displacements of the lower catenary 4, the axial fluctuating displacements of lower head sheave 4 were recorded by using inductive displacement transducer as shown in Figure 15. The inductive displacement transducers fixed in the retainer were adjusted to face the outer rim of the sheaves. Employing fast Fourier transform, the amplitude spectrum of the axial fluctuating displacements of lower head sheave 4 can be obtained as shown in Figure 16.

4.2. Validation. It can be seen from Figure 16 that the first three-order frequency components play the dominating roles in the axial fluctuating displacements of the head sheave. Thus, the external displacement excitations at the sheave end of the lower hoisting catenary 4 can be specified by $1.46\sin(wt)$ mm, $6.1\sin(2wt)$ mm, and $2.1\sin(3wt)$ mm, respectively, where w is the fundamental angular frequency of the head sheave. Under the above external excitations, according to (31) and employing the corresponding parameters introduced in Section 3.2, the time histories of transverse displacements at the center of lower catenary 4 under no and full hoisting load were given in Figures 17 and 18, respectively.

Under the circumstance of full hoisting load with m_p = 20000 kg, it can be seen from Figure 17 that the first-order response amplitude is much smaller than the second- and third-order amplitudes and thereby can be negligible.

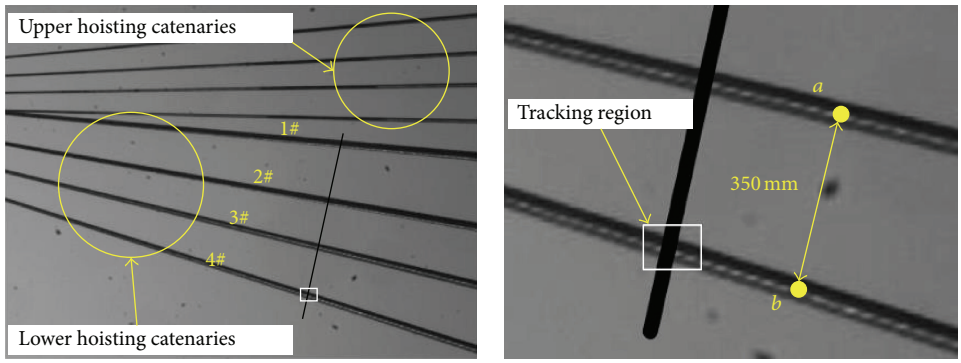

(a) (b)

Figure 13: The processed image: (a) the global image and (b) the local image.

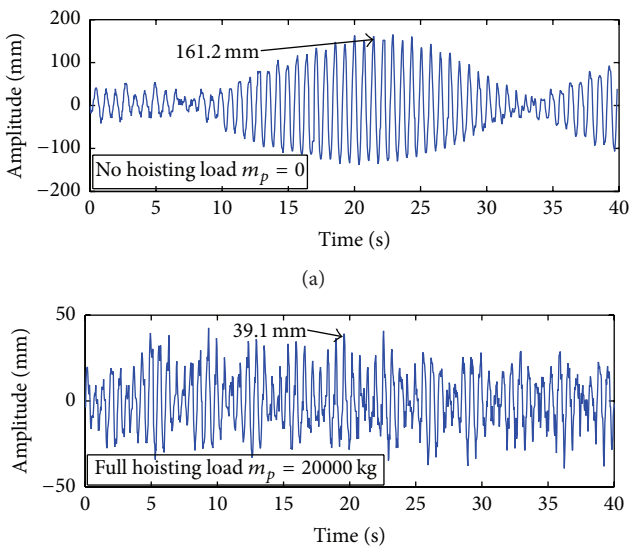

Figure 14: Transverse vibration displacements at the center of the lower catenary 4: (a) no load, $m_p = 0$, and (b) full load, $m_p = 20000$ kg.

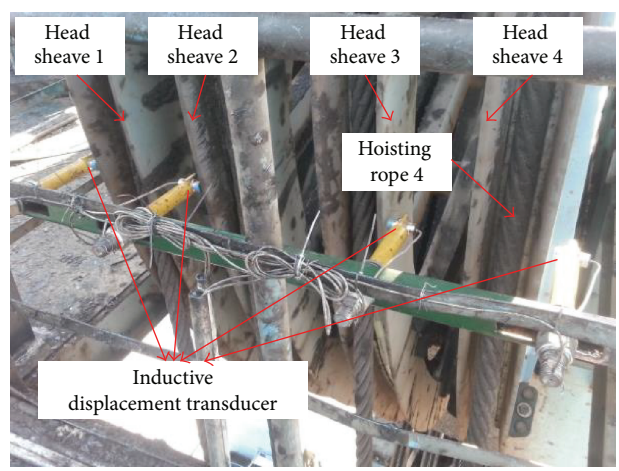

Figure 15: Measurement of the axial fluctuating displacements of head sheaves.

The maximum values of the second- and third-order response amplitude in Figure 17 are 28.96 mm and 10.1 mm, respectively. According to superposition principle, the sum of the second- and third-order maximum amplitudes is 39.06 mm, which is much close to the measured 39.1 mm shown in Figure 14. Furthermore, the shapes of the vibrating waveforms under the second- and third-order excitations in Figure 17, especially the second-order excitation, are similar to the measured shapes as shown in Figure 14.

Under the circumstance of no hoisting load, it can be seen from Figure 18 that the first- and third-order response amplitudes are much smaller than the second-order response amplitude and thereby can be negligible. The maximum value of the second-order response amplitude in Figure 18 is 155.6 mm, which is much close to the measured 161.2 mm shown in Figure 14. Additionally, the shape of the vibrating waveform under the second-order excitation in Figure 18 is similar to the measured shape as shown in Figure 14.

Figures 14 and 18 are interesting since experimental and numerical time histories are similar and present "beat." These seem associated mainly with the second-order excitation. To account for this issue, under the condition of no load, the corresponding amplitude spectrum of Figure 14(a) was given in Figure 19(a). It can be seen that the main vibration frequency is 1.36 Hz relating to the lower catenary 4. The hoisting velocity during the constant speed stage is 9.31 m/s; therefore, the fundamental excitation frequency can be obtained as 0.66 Hz by calculating the rotational frequency. It can be noted that the second-order excitation frequency of 1.32 Hz is much close to 1.36 Hz, the measured vibration frequency. Therefore, it can be concluded that the second-order excitation frequency is the main excitation frequency. To more clearly and accurately account for this issue, by varying the excitation frequency under the excitation $0.005\sin(wt)$, the maximum transverse amplitudes at the center of a catenary are depicted as shown in Figure 19(b). It can be got that the second-order excitation angular frequency of 8.28 rad/s is

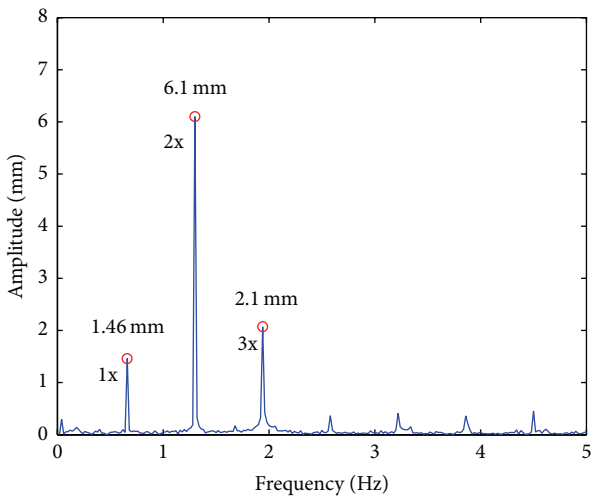

FIGURE 16: Amplitude spectrum of axial fluctuations of lower head sheave 4.

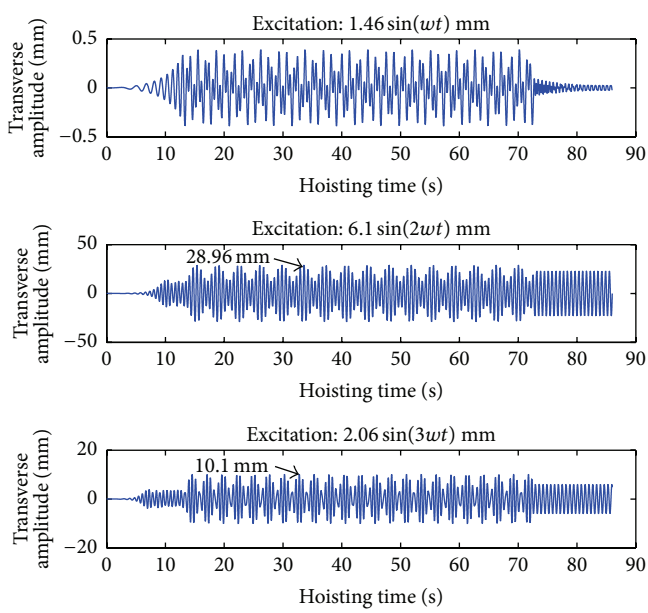

FIGURE 17: Simulation of transverse vibrations at the center of lower catenary 4 under the condition of full hoisting load.

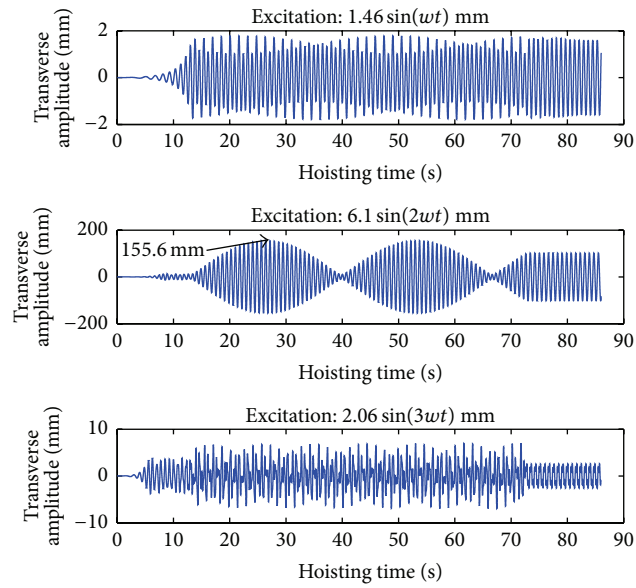

FIGURE 18: Simulation of transverse vibrations at the center of lower catenary 4 under the condition of no hoisting load.

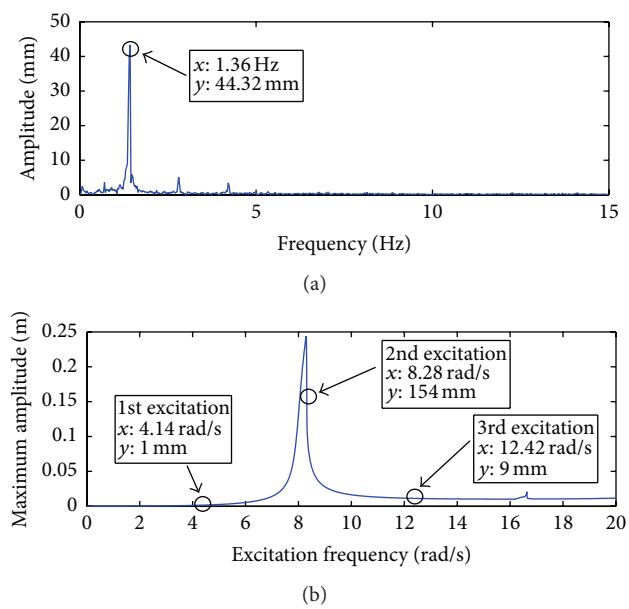

FIGURE 19: (a) Amplitude spectrum corresponding to lower catenary 4 and (b) amplitude-frequency curve of the transverse vibrations in a catenary.

closer to the resonance frequency than the first- and third-order and the "beat" thereby resulted.

Some differences may result from model errors, which are acceptable when the primary purpose is fault diagnosis. In conclusion, the validity and applicability of the dynamic model and governing equation of the transverse vibrations of hoisting catenaries can be confirmed. Most important of all, the accuracy of the effect of hoisting load on transverse vibrations of hoisting catenaries can be validated, providing reasonable basis for the optimization of the hoisting load and even great help during the design phrase of the machine.

5. Conclusions

The dynamics of the vertical translating hoisting rope is particularly focused on in the present study. The theoretical model and numerical solution scheme provide an efficient approach to analyzing the transverse and longitudinal coupled vibrations of the vertical translating hoisting rope. The simulation results indicate that the transverse vibration plays the dominating role in the coupled dynamics of the vertical hoisting rope subjected to external excitation induced by axial

fluctuations of the head sheave, and the rope tension can be approximated by the quasistatic tension.

According to the quasistatic tension of the hoisting rope, the effects of hoisting load on the transverse vibrations of the hoisting catenary were discussed employing dynamic simulations during lifting. Under the second-order excitation frequency, a discrepant large transverse amplitude will be excited when the hoisting load ranges from 0 to 5000 kg. Therefore, collision between two adjacent catenaries will result and the rupture of the rope will be thereby accelerated. To solve this problem, the self-weight of the conveyance (preload) can be optimized from 39500 kg to 49500 kg by adding 10000 kg according to the simulation curves.

On-site measurements were performed on the studied multirope friction hoist in coal mines. The simulation results were well consistent with the practically measured results, confirming the validity and applicability of the dynamic model and governing equation of the transverse vibrations of hoisting catenaries and validating the accuracy of the effect of hoisting load on transverse vibrations of hoisting catenaries.

Eventually, this investigation will provide great theoretical basis to realize resonance avoidance of the hoisting catenaries by optimizing the hoisting load in a multirope friction mine hoist. Furthermore, the research results will also be a great help during the design phrase of the machine.

Conflict of Interests

The authors declare that there is no conflict of interests regarding the publication of this paper.

Acknowledgments

The authors gratefully acknowledge the support of National Natural Science Foundation of China (Grant no. 51375479). The authors gratefully acknowledge the support of a Project Funded by the Priority Academic Program Development of Jiangsu Higher Education Institutions (PAPD).

References

[1] D. G. Wang, D. K. Zhang, and S. R. Ge, "Determination of fretting parameters of hoisting rope in coalmine and fretting-fatigue behavior of steel wires," *Industrial Lubrication & Tribology*, vol. 65, no. 6, pp. 436–448, 2013.

[2] Y. Liu, G. D. Chen, J. H. Li, and Y. J. Xue, "Dynamics simulation of the hoisting cable of single cable winding hoisting device," *Mechanical Science and Technology for Aerospace Engineering*, vol. 28, no. 9, pp. 1225–1229, 2009.

[3] G. H. Cao, Z. C. Zhu, W. H. Peng, and X. G. Shao, "Coupled extensional-torsional vibration frequency of hoisting rope in tower-type friction drive hoist system," in *Proceedings of the International Conference on Measuring Technology and Mechatronics Automation (ICMTMA '09)*, pp. 615–618, IEEE, Hunan, China, April 2009.

[4] G. H. Cao, Z. C. Zhu, W. H. Peng, and X. B. Mao, "Modeling and natural frequency characteristics of coupled vibration with varying length of hoisting rope in drum winding system," in *Proceedings of the International Conference on Computing, Control and Industrial Engineering (CCIE '10)*, pp. 367–370, IEEE, Wuhan, China, June 2010.

[5] J. J. Wang, G. H. Cao, Z. C. Zhu, Y. D. Wang, and W. H. Peng, "Lateral response of cable-guided hoisting system with time-varying length: theoretical model and dynamics simulation verification," *Proceedings of the Institution of Mechanical Engineers, Part C: Journal of Mechanical Engineering Science*, vol. 229, no. 16, pp. 2908–2920, 2015.

[6] O. A. Goroshko, "Evolution of the dynamic theory of hoist ropes," *International Applied Mechanics*, vol. 43, no. 1, pp. 64–67, 2007.

[7] G. F. Gong, "Analysis of the string vibration for mine hoist," *Mining Machinery*, vol. 12, pp. 48–50, 1990.

[8] S. Kaczmarczyk, "The passage through resonance in a catenary-vertical cable hoisting system with slowly varying length," *Journal of Sound and Vibration*, vol. 208, no. 2, pp. 243–269, 1997.

[9] S. Kaczmarczyk and W. Ostachowicz, "Transient vibration phenomena in deep mine hoisting cables. Part 1: mathematical model," *Journal of Sound & Vibration*, vol. 262, no. 2, pp. 219–244, 2003.

[10] S. Kaczmarczyk and W. Ostachowicz, "Transient vibration phenomena in deep mine hoisting cables. Part 2: numerical simulation of the dynamic response," *Journal of Sound & Vibration*, vol. 262, no. 2, pp. 245–289, 2003.

[11] R. R. Mankowski and F. J. Cox, "Response of mine hoisting cables to longitudinal shock loads," *Journal of The South African Institute of Mining and Metallurgy*, vol. 86, no. 2, pp. 51–60, 1986.

[12] D. G. Wang, D. K. Zhang, and S. R. Ge, "Effect of terminal mass on fretting and fatigue parameters of a hoisting rope during a lifting cycle in coal mine," *Engineering Failure Analysis*, vol. 36, pp. 407–422, 2014.

[13] P. Wang, X. M. Xiao, B. H. Ding, and S. B. Li, "Dynamic simulation of wire rope of mine hoist in lifting process," *Hoisting Conveyance Machinery*, vol. 7, pp. 84–87, 2009.

[14] W. D. Zhu and H. Ren, "An accurate spatial discretization and substructure method with application to moving elevator cable-car systems-part I: methodology," *Journal of Vibration and Acoustics—Transactions of the ASME*, vol. 135, no. 5, Article ID 051036, pp. 1–10, 2013.

[15] P. Zhang, C.-M. Zhu, and L.-J. Zhang, "Analysis of forced coupled longitudinal-transverse vibration of flexible hoisting systems with varying length," *Engineering Mechanics*, vol. 25, no. 12, pp. 202–207, 2008.

[16] W. D. Zhu and Y. Chen, "Forced response of translating media with variable length and tension: application to high-speed elevators," *Proceedings of the Institution of Mechanical Engineers Part K: Journal of Multi-Body Dynamics*, vol. 219, no. 1, pp. 35–53, 2005.

[17] H. Ren and W. D. Zhu, "An accurate spatial discretization and substructure method with application to moving elevator cable-car systems—part II: application," *Journal of Vibration & Acoustics*, vol. 135, no. 5, Article ID 051037, 21 pages, 2013.

[18] E. V. Kurmyshev, "Transverse and longitudinal mode coupling in a free vibrating soft string," *Physics Letters A*, vol. 310, no. 2-3, pp. 148–160, 2003.

[19] J. N. Yao, X. M. Xiao, A. H. Peng, Y. Q. Jiang, and C. Ma, "Assessment of safety for axial fluctuations of head sheaves in mine hoist based on coupled dynamic model," *Engineering Failure Analysis*, vol. 51, pp. 98–107, 2015.

[20] D. Comaniciu, V. Ramesh, and P. Meer, "Kernel-based object tracking," *IEEE Transactions on Pattern Analysis and Machine Intelligence*, vol. 25, no. 5, pp. 564–577, 2003.

[21] Y. Cheng, "Mean shift, mode seeking, and clustering," *IEEE Transactions on Pattern Analysis and Machine Intelligence*, vol. 17, no. 8, pp. 790–799, 1995.

[22] K. Nummiaro, E. Koller-Meier, and L. V. Gool, "Color features for tracking non-rigid objects," *Acta Automatica Sinica*, vol. 29, no. 3, pp. 345–355, 2003.

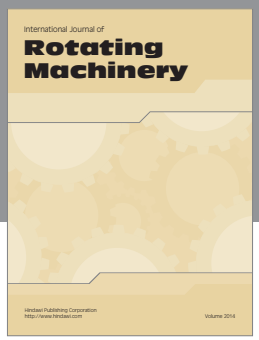

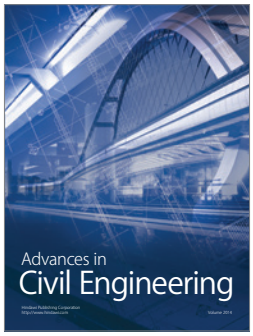

Hindawi

Submit your manuscripts at
http://www.hindawi.com